The Andes Affect ENSO Statistics

WEIXUAN XU,[a] JUNG-EUN LEE,[a] BAYLOR FOX-KEMPER,[a] YANN PLANTON,[b] AND MICHAEL J. MCPHADEN[b]

[a] *Department of Earth, Environmental and Planetary Sciences, Brown University, Providence, Rhode Island*
[b] *Pacific Marine Environmental Laboratory, NOAA, Seattle, Washington*

(Manuscript received 9 November 2021, in final form 9 June 2022)

ABSTRACT: Current coupled global climate models have biases in their simulations of the tropical Pacific mean-state conditions as well as the El Niño–Southern Oscillation (ENSO) phenomenon. Specifically, in the Community Earth System Model (CESM version 1.2.2), the tropical Pacific mean state has overly weak sea surface temperature (SST) gradients in both the zonal and meridional directions, ENSO is too strong and too regular, and El Niño and La Niña events are too symmetrical. A previous study with a slab-ocean model showed that a higher elevation of the Andes can improve the tropical Pacific mean-state simulation by adjusting the atmospheric circulation and increasing the east–west and north–south SST gradients. Motivated by the link between the mean tropical Pacific climate and ENSO variations shown in previous studies, here we explored the influence of the Andes on the simulation of ENSO using the CESM 1.2.2 under full atmosphere–ocean coupling. In addition to improving the simulated tropical Pacific mean state by increasing the strength of the surface easterly and cross-equatorial southerly winds, the Higher Andes experiment decreases the amplitude of ENSO, increases the phase asymmetry, and makes ENSO events less regular, resulting in a simulated ENSO that is more consistent with observations. The weaker ENSO cycle is related to stronger damping in the Higher Andes experiment according to an analysis of the Bjerknes index. Our overall results suggest that increasing the height of the Andes reduces biases in the mean state and improves the representation of ENSO in the tropical Pacific.

KEYWORDS: ENSO; Atmosphere-ocean interaction; Model errors; Interannual variability

1. Introduction

The tropical Pacific climate is formed by the large-scale interaction between the atmosphere and the ocean. Its mean state has strong contrast between the wet and warm western Pacific and the cold and dry eastern Pacific. Deviating from this mean state, the tropical Pacific climate has a natural interannual variation called El Niño–Southern Oscillation [ENSO; see McPhaden et al. (2020) for a review]. ENSO events alter the global atmospheric circulation, causing unusual floods or droughts to occur in many regions (e.g., Prieto 2007), creating threats to our society in many aspects including agriculture (Nicholls 1991), fisheries (Lehodey et al. 2020), public safety (Fang et al. 2021), and economic vitality (Bastianin et al. 2018).

Due to ENSO's impacts, understanding its dynamics and predicting it a few seasons in advance has been the focus of intensive research over the last 50 years. Early methods built simplified models to simulate the components that affect ENSO's initiation, generation, and dissipation (e.g., Bjerknes 1969; Wyrtki 1985; Cane and Zebiak 1985; Jin 1996, 1997a,b). These simplified climate models do simulate a quasi-periodic signal and reveal some of the key components of the ENSO cycle, but many important aspects of ENSO are not accounted for. With the lack of seasonal modulation and the nonlinear processes in these simplified models, they are too limited in scope and cannot reproduce the full complexity and diversity of ENSO (Jin et al. 2020; Levine et al. 2016). Coupled global circulation models (CGCMs) are better suited to capture many characteristics of ENSO compared with simplified models, but they still have a lot of systematic errors (Guilyardi et al. 2009; Bellenger et al. 2014; Guilyardi et al. 2020; Planton et al. 2021), including biases in the mean state, in processes contributing to the growth and decay of ENSO and occurrence statistics. Biases in the mean state include the SST distribution, double intertropical convergence zone (ITCZ) bias, and the errors in surface wind simulation (e.g., Guilyardi et al. 2020; Planton et al. 2021). Biases in ENSO properties include the wrong amplitude, too sharply peaked power spectrum, excess westward displacement of the ENSO pattern, too little skewness, and so on (e.g., Guilyardi et al. 2020; Planton et al. 2021). In addition, there are still considerable uncertainties in ENSO properties under a warmer climate, although climate models are improving in the agreement of future projections (Cai et al. 2018, 2021).

Progress in overcoming these difficulties has taken many forms. One solution is increasing the spatial and temporal resolutions of the atmosphere and ocean models (Wittenberg et al. 2018). However, it is a slow and challenging process to reach higher-resolution model simulations, since each increase in resolution is exponentially more difficult. Fox-Kemper et al. (2014) showed that the past decades' rate of computational improvement results in the doubling of full-complexity CGCM resolution only every 10.2 years [consistent with a recent update by Haine et al. (2021)]. Therefore, instead of using a higher-resolution climate model, we attempt to

Denotes content that is immediately available upon publication as open access.

Corresponding author: Weixuan Xu, weixuan_xu@brown.edu

DOI: 10.1175/JCLI-D-21-0866.1

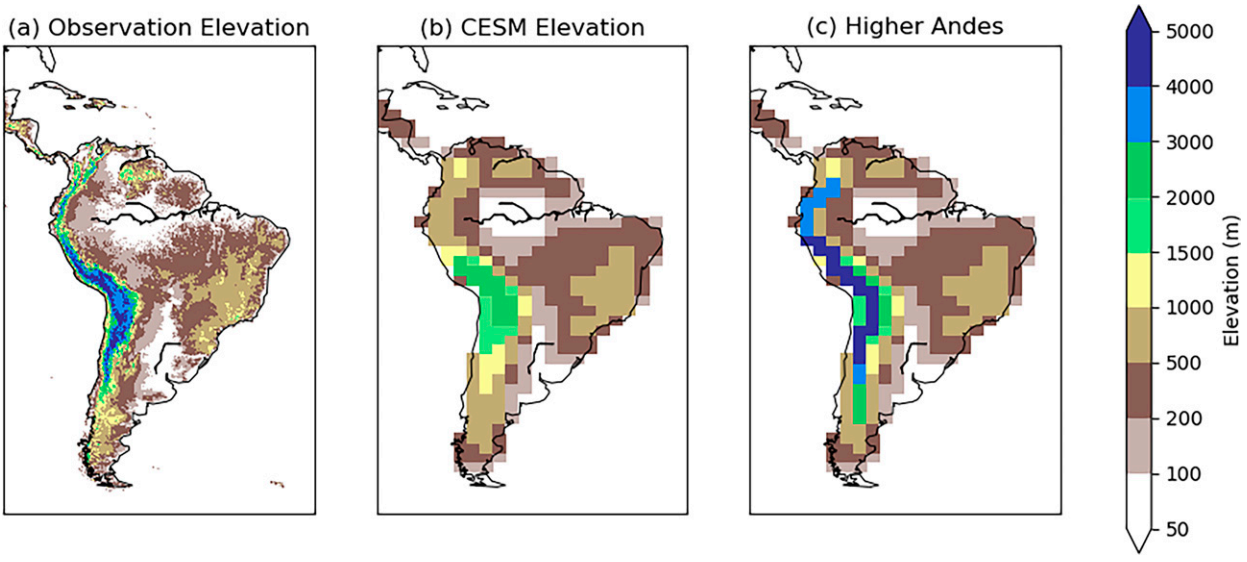

FIG. 1. Elevation in South America from (a) National Oceanic and Atmospheric Administration (NOAA) National Geophysical Data Center (NGDC) Global Land One-km Base Elevation (GLOBE) topography, (b) 1.9° × 2.5° resolution of CESM Control experiment topography, and (c) Higher Andes experiment topography. The height of the Andes is adjusted to the highest value according to the GLOBE topography: In each coarse-grained grid cell along the Andes in the climate model, we computed its elevation as the maximal elevation within the cell area of the fine-grained observations. This figure is the same as Fig. 1 in Xu and Lee (2021).

improve ENSO simulations by better representing dynamical processes.

As many errors in ENSO properties and errors in the mean-state climate are closely connected (e.g., Zhang and Sun 2014; Abellán et al. 2017; He et al. 2018), adjustments that can improve the mean-state simulations may also improve the ENSO simulation. The mean state over the Pacific can be influenced by many aspects of the modeling system, but the focus in this paper is the representation of the Andes. Previous studies showed that removing all orography in a CGCM modulates the mean states and ENSO has a stronger amplitude and increased regularity (Kitoh 2007; Naiman et al. 2017). As the Andes alone are important for the formation of the southeast Pacific cold tongue (Takahashi and Battisti 2007), Xu and Lee (2021) hypothesized that the Andes are not high enough in the low-resolution CGCMs and improving that could improve the simulation of the Pacific mean state and variability. Indeed, with too low Andes, the modeled range insufficiently modulates the atmospheric circulation and results in too warm SST in the southeast Pacific and too much precipitation over the South Pacific. To test this hypothesis, Xu and Lee (2021) modified the Andes in a coupled system with a slab-ocean model and compared the experiment with a higher elevation of the Andes model versus a control experiment with the standard coarsened Andes orography. They found an improvement in the simulation of the tropical Pacific mean state with lowered SST in the southeast Pacific cold tongue and the inhibition of precipitation over the central South Pacific. We hypothesize that modifying the Andes will affect ENSO as well.

In this paper, we explore whether modification of the Andes can improve simulations of the mean-state climate and the ENSO cycle in the tropical Pacific using a CGCM, focusing on the role of upper-ocean dynamical feedbacks. Section 2 introduces the experimental setup and the model setting. Sections 3 and 4 compare the model results in terms of the mean state and ENSO cycle. Section 5 discusses the mechanism explanations of our result and section 6 talks about its scientific importance.

2. Method

a. Model and experiment

We used the National Center for Atmospheric Research (NCAR) Community Earth System Model (CESM) version 1.2.2 (Hurrell et al. 2013). It includes the Community Atmospheric Model, version 4 (CAM4), as the atmosphere component, and an extension of the Parallel Ocean Program (POP) version 2 from Los Alamos National Laboratory (LANL) as the ocean component. We ran the model with CO_2 concentration as in year 2000 (367 ppm) so that we can compare our result with the satellite data. We used the atmospheric resolution of 1.9° × 2.5° with 26 vertical layers and nominal oceanic resolution of 1° with 60 vertical layers for our experiment.

Boos and Kuang (2010) showed that the narrow Himalayan mountain ranges, rather than the Tibetan Plateau, is essential to modulate the South Asian monsoon. Inspired by their study, we consider the Andes as a similar barrier that influences the topical Pacific circulations. Figure 1a shows the 1-km high-resolution topography from the National Oceanic and Atmospheric Administration (NOAA) National Geophysical Data Center (NGDC) Global Land One-km Base Elevation (GLOBE) topography, and Fig. 1b is the default topography setting in CESM (used in our control experiment). To

understand the influence from the Andes, we modified the height of the Andes to the highest value according to the GLOBE topography (Fig. 1c; experiment called "Higher Andes"). In each coarse-grained grid cell along the Andes in the climate model, we computed its elevation as the maximal elevation within the cell area of the fine-grained observations. Our approach is to evaluate the maximum possible influence of the Andes, and not to simulate the exact influence of the Andes. Both experiments were run for 350 years to allow the upper ocean to adjust to the modification, and we used the last 160 years of model output for our analysis.

b. Analysis

To analyze the model performance, we used the ENSO metrics package developed by the International Climate and Ocean: Variability, Predictability and Change (CLIVAR) Pacific region panel (Planton et al. 2021). These metrics allow us to rapidly diagnose and evaluate the model's performance regarding the ENSO-related mean state and properties, teleconnection pattern, and dynamical coupling. In this research, we will focus on the comparison of the simulation accuracy between the Control and Higher Andes experiments.

To evaluate the model's performance on the tropical Pacific climate, we use HadISST's SST (Rayner et al. 2003), GPCPv2.3's precipitation (Adler et al. 2003), TropFlux's net surface heat fluxes and surface wind stress (Praveen Kumar et al. 2012, 2013), and the Met Office Hadley Centre's EN4 ocean temperature profile (Good et al. 2013). We use monthly data from these products over the period 1979–2018. Although the CO_2 forcing within this period is not constant as in the model, it increases linearly with the average value approximately equal to that in year 2000. Therefore we still consider it a fair comparison.

To compare the spatial distributions between the observations and the simulations, all data are interpolated onto a regular $1^\circ \times 1^\circ$ grid. The gridded observational datasets available are not perfect and choosing another group of datasets may slightly change the metric values (e.g., Planton et al. 2021). Using these observational datasets we do not precisely evaluate the model, but merely detect the differences between the Control and Higher Andes experiments and estimate if the new simulation is getting better or worse.

In the evaluation of the mean-state distribution (Figs. 2, 4, and 5), the model mean distributions are calculated from averaging the 160-yr model results. To make comparisons with the 40 years of observation data, the error bars are calculated using the bootstrapping method. We did 10 000 bootstrapping samples each selecting 480 months of data (i.e., 40 years) and calculated the average distribution of each sample. The error bars are calculated as the standard deviation over the 10 000 40-yr-equivalent averages. The distribution of the 10 000 averages is nearly Gaussian, so the standard deviation is an adequate measure of uncertainty.

For the ENSO variations section (Figs. 7, 8, and 10), unlike the mean-state uncertainties, the ENSO variations are interannual signals continuous in time. Their spectral analysis is most meaningful within a continuous decadal-scale period matching in duration to the available observational data. Thus, the 160 years of model results are divided into four nonoverlapping sections of 40 continuous years. Corresponding distributions of each section are plotted as the thin light lines, and the averaged values of the four sections are plotted as the thick dark lines. Root-mean square errors (RMSEs) are calculated between the averaged distributions and the observations.

To quantify the processes that influence the ENSO variation, we calculated the Bjerknes stability index (Jin et al. 2006) with the same equation as Zhao and Fedorov (2020):

$$2I_{\mathrm{BJ}} = -\alpha_s - \frac{\langle \overline{u} \rangle}{L_x} - \frac{\langle -2y\overline{v} \rangle}{L_y^2} - \frac{\langle \mathcal{H}(\overline{w})\overline{w} \rangle}{H_m} + \mu_a \beta_u \left\langle \frac{\partial \overline{T}}{\partial x} \right\rangle + \mu_a \beta_w \left\langle \frac{\partial \overline{T}}{\partial z} \right\rangle + \mu_a \beta_h a_h \left\langle \frac{\overline{w}}{H_m} \right\rangle. \quad (1)$$

The terms on the right-hand side of this equation are as follows: term 1 is thermal damping (TD); terms 2, 3, and 4 together add up as the mean advection damping (MA); term 5 is zonal advection feedback (ZA); term 6 is Ekman feedback (EK); and term 7 is thermocline feedback (TH). The first two mechanisms act as a damping effect on ENSO, while the remaining three feedback processes strengthen ENSO. This equation separates the different mechanisms that can influence the ENSO cycle, which allows us to understand the key processes by which the Higher Andes experiment differs from the control experiment.

3. Changes in the mean state

Similar to the slab-ocean model simulations (Xu and Lee 2021), the Higher Andes in the atmosphere–ocean coupled model changes the mean state of the ocean and atmosphere. We will evaluate these changes in four aspects related to mean changes usually taken to affect ENSO: SST, precipitation, wind stress, and ocean stratification.

a. SST and precipitation

Bayr et al. (2018) and Wengel et al. (2018) found a link between the mean SST bias and ENSO seasonality as well as the balance of mechanisms generating SST anomalies. As SST and precipitation biases are linked (e.g., Oueslati and Bellon 2015; Brown et al. 2020), the effect of the height of the Andes on these biases is also analyzed in this section.

Figure 2 shows the latitudinal and longitudinal distribution of SST and precipitation in the observation (black line), Control (red line), and Higher Andes experiments (blue line). In the eastern Pacific (Fig. 2a), the SST across latitudes is too warm in both experiments, but this warm bias is smaller in the Higher Andes experiment than in the Control experiment (RMSE of 0.6° and 1.2°C, respectively), especially south of the equator. As a consequence, the north–south (N–S) SST gradient (defined as the difference between the highest SST in the Northern and Southern Hemispheres) is better reproduced in the Higher Andes experiment than in the Control experiment (Higher Andes: 1.4°C; Control: 0.7°C; observation:

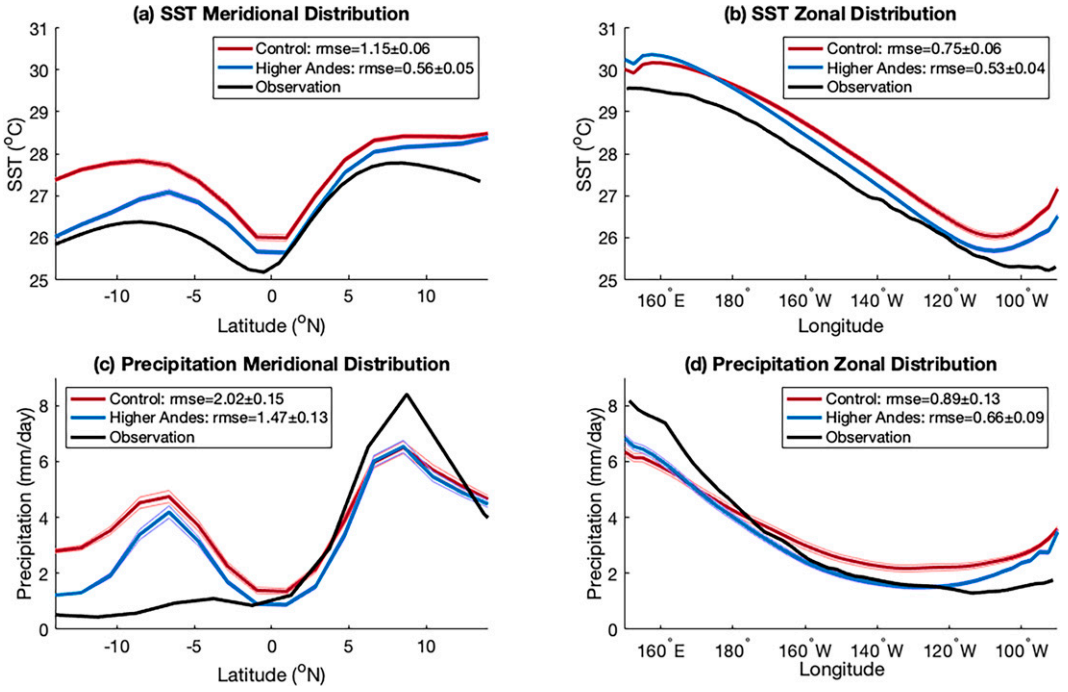

FIG. 2. (a),(b) SST distribution in observation, Control, and Higher Andes experiments (°C) and (c),(d) precipitation distribution in observation, Control, and Higher Andes experiments (mm day^{-1}), showing distributions (a),(c) across latitudes (zonal average: 150°E–90°W) and (b),(d) along the equator (meridional average: 5°S–5°N). The solid lines in model results are the averaged distribution over 160 years. The error bars are calculated with the bootstrapping method. We did 10 000 times of bootstrapping with 480 months (40 years) of data, and calculated the average distribution of each bootstrapping samples. The error bars are the standard deviations of these 10 000 average distributions. The observation distributions (black lines) are the average distribution of 40 years. The legends also show the root-mean-square errors (RMSEs) calculated as the averaged difference between the model mean values (blue and red solid lines) and observations (black solid line). Uncertainties of the RMSEs are the averaged values of the error bars. See section 2 for detailed explanations.

1.5°C). Both experiments are also too warm along the equator (Fig. 2b), but again the bias is reduced in the Higher Andes experiment compared to the Control experiment (RMSE of 0.5° and 0.8°C, respectively). Note that the bias is reduced everywhere but west of the date line.

In the tropical Pacific, the air from the Southern and Northern Hemispheres converges. The converged air is forced upward and creates the intertropical convergence zone (ITCZ), a region of heavy precipitation, on average located at the north of the equator (Philander et al. 1996). The observed precipitation distribution across latitudes in the eastern Pacific (Fig. 2c; black line) displays a strong N–S precipitation difference, with around 1 mm day^{-1} south of the equator and a peak reaching 8 mm day^{-1} around 7°N. In both experiments, the distribution of precipitation is too symmetric with respect to the equator, a persistent error in climate models called the double ITCZs bias (e.g., Lin 2007; Bellenger et al. 2014; Planton et al. 2021). The section-averaged bias is around 2.0 mm day^{-1} in the Control experiment (red line), and the N–S precipitation gradient (defined as the difference between the largest precipitation in the Northern and Southern Hemisphere) is around 2.1 mm day^{-1}. In the Higher Andes experiment, the double ITCZ bias is still present but reduced (the N–S precipitation difference of 2.4 mm day^{-1}), slightly reducing the mean bias (1.5 mm day^{-1}). However, increasing the height of the Andes does not improve the dry bias in the western equatorial Pacific, as shown in Fig. 2d. But it inhibits central and eastern tropical Pacific precipitation and still reduces the total precipitation bias (RMSE of 0.9 mm day^{-1} in the Control experiment and of 0.7 mm day^{-1} in the Higher Andes experiment).

The changes brought by the modification of the Andes are similar in the present experiment with a fully coupled climate model and in the experiment from Xu and Lee (2021) with a slab-ocean model (Fig. 3): a higher elevation of the Andes setting lowers the SST and reduces precipitation over the eastern tropical Pacific area. However, the difference between the Control and the Higher Andes experiments is smaller in the fully coupled climate model, which means that the ocean circulation feedbacks respond to withstand the changes in the atmosphere, and end up weakening the influence from the Andes.

b. *Wind stress*

The surface wind over the tropical Pacific is an important factor that influences the heat and moisture transport, controls the coastal upwelling, and contributes to the development of the ENSO cycle (McPhaden et al. 2020). As both zonal and

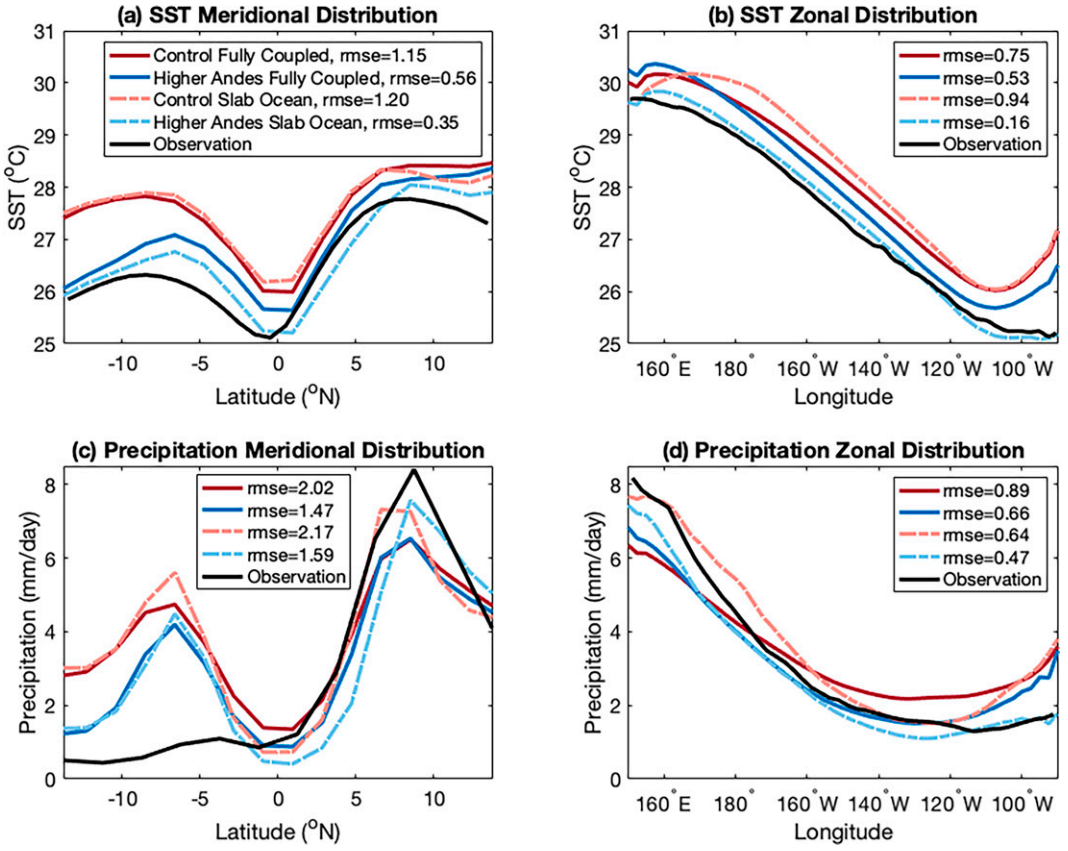

FIG. 3. As in Fig. 2, but for the comparison between fully coupled model results (thick solid lines) and slab-ocean model results (thin dashed lines). The modeled fully coupled distributions are averaged over the last 160 years of 350 years simulations. The slab-ocean distributions are averaged over the last 10 years of 30-yr simulations. Here we only showed the average distributions but not the error bars because the fully coupled experiments and the slab-ocean experiments are run for different lengths compared with the observation. The legends also show the RMSEs calculated between the each modeled average values and observations.

meridional wind stress modulate the amplitude of ENSO events (Hu and Fedorov 2018; Zhao and Fedorov 2020), we analyze their evolution between the two experiments in this section (Fig. 4).

The tropical Pacific region, zonal wind stress is, on average, from east to west along the equator in the Pacific. The meridional component is northward in the Southern Hemisphere and up to 7°N and southward in higher latitudes, to form the ITCZ (Fig. 4, black lines). This pattern is well reproduced in the Control experiment, but the cross-equatorial winds in the eastern equatorial Pacific are too weak (they reach 30×10^{-3} N m^{-2} in the observation, but only 12×10^{-3} N m^{-2} in the Control experiment; Fig. 4d).

With the Higher Andes experiment, zonal wind stress becomes stronger than in the Control experiment and observations in the South Pacific (Fig. 4a) and in the central to western Pacific region (Fig. 4b), and becomes weaker in the eastern Pacific region (Fig. 4b). As a consequence, the zonal wind stress biases are slightly larger in the Higher Andes experiment than in the Control experiment, across latitudes (4.5×10^{-3} and 2.7×10^{-3} N m^{-2} respectively) and along the equator (11.0×10^{-3} and 6.7×10^{-3} N m^{-2} respectively). The meridional component does not change much across latitudes (Fig. 4c). It becomes slightly too strong south of 5°S in the Higher Andes experiment and gets closer to the observation in the equatorial band (5°S–5°N). This does not change the mean bias much (from 4.7×10^{-3} N m^{-2} in the Control experiment to 3.0×10^{-3} N m^{-2} in the Higher Andes experiment). Along the equator (Fig. 4d), there is little change west of 200°E, but in the eastern equatorial Pacific, the cross-equatorial winds are strengthened in the Higher Andes experiment, getting closer to the observation (but still too weak). This bias is slightly improved but not by a lot (around 11.5×10^{-3} N m^{-2} in the Control experiment and around 8.9×10^{-3} N m^{-2} in the Higher Andes experiment).

The modified atmospheric circulation is related to the change in SST. Similar to the slab-ocean model results from Xu and Lee (2021) (Fig. 3), the Higher Andes experiment lowers the SST in the southeast Pacific by enhanced evaporative and radiative cooling (Xu and Lee 2021). The cooler SST in the South Pacific will enhance the high sea surface pressure in the subtropical South Pacific, and therefore enhance the anticyclonic

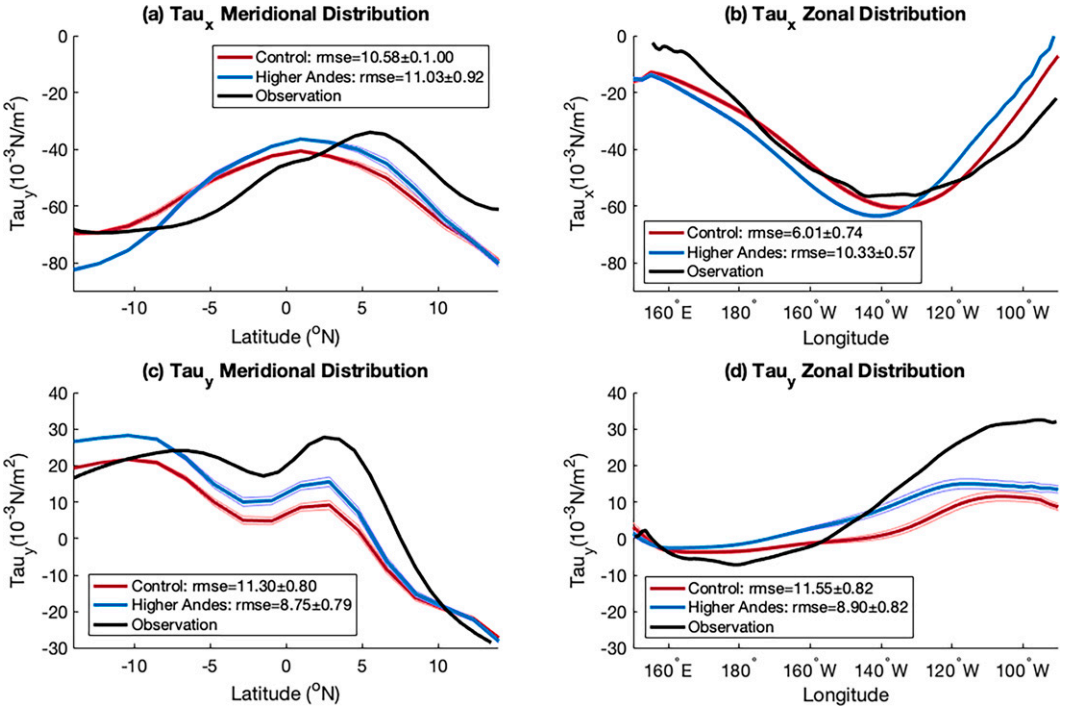

FIG. 4. As in Fig. 2, but for the zonal and meridional wind stress (10^{-3} N m^{-2}). In (a) and (c), the zonal average is computed between 150°E and 90°W.

motion (Takahashi and Battisti 2007). This enhanced anticyclonic motion includes stronger easterly winds in the western equatorial Pacific (Fig. 4b). Also, the colder SST in the South Pacific increases the surface pressure gradient in the south and the North Pacific, forming a stronger cross-equatorial wind from the Southern Hemisphere to the Northern Hemisphere (Fig. 4c). In conclusion, imposing a higher elevation of the Andes induces stronger zonal and meridional wind stress in the tropical Pacific.

SST biases in different climate models are different (e.g., Fig. 2 in Burls et al. 2017), but one common problem is that the east–west SST gradient in the climate models is too small. The biases are either a warm bias or a weaker cold bias in the eastern Pacific, indicating that the SST gradient in most of the CMIP5 models is not as strong as in the observations. Our experiment increases the east–west SST gradient by elevating the height of the Andes, and this change is accompanied by stronger winds over the tropical Pacific.

c. *Ocean stratification*

Because the Higher Andes setting changes the atmosphere circulation, the upper ocean would respond to this change and reach a new equilibrium. Here we show the upper-ocean temperature distribution in the two experiments from years 191 to 350. An important aspect of the signal that develops into an ENSO event is the propagation of a temperature anomaly in the subsurface ocean, and it can be measured by the change of thermocline depth (e.g., Zhao and Fedorov 2020).

Figure 5 shows the potential temperature distribution in the Niño-3 region (5°S–5°N, 150°–90°W) in both experiments and in the observations (left panel), as well as the differences between the model and the observations (right panel). The Higher Andes experiment is closer to the observations, being colder than the Control experiment in the upper 150 m and warmer than the Control experiment from 150 to 300 m. As shown in Fig. 5, compared with the Higher Andes experiment, the Control experiment has a too large vertical temperature gradient in the Niño-3 region, implying too strong stratification.

Figures 6a and 6b show the vertical distribution and the change of potential temperature in the upper ocean of the equatorial Pacific. The thermocline in the Pacific Ocean is tilted (black line in Fig. 6a); it is deeper in the western Pacific and shallower in the eastern Pacific. A cooler potential temperature indicates a shallower thermocline, while a warmer potential temperature indicates a deeper thermocline. The Higher Andes experiment imposes a cooling in the eastern part of the thermocline, and a warming in the western part (Fig. 6b), indicating a shallower thermocline in the east and deeper in the west, resulting in a more zonal thermocline tilt.

However, this change in upper-ocean potential temperature is not driven by stronger coastal upwelling. In the eastern equatorial Pacific, the upper ocean is dominated by strong upward motion (Fig. 6c), but in the Higher Andes, upwelling weakens due to the weaker zonal wind stress in the eastern Pacific (Fig. 4b).

4. Changes in ENSO properties

As the mean-state climate over the tropical Pacific is thought to be related to the ENSO variability (Zhao and

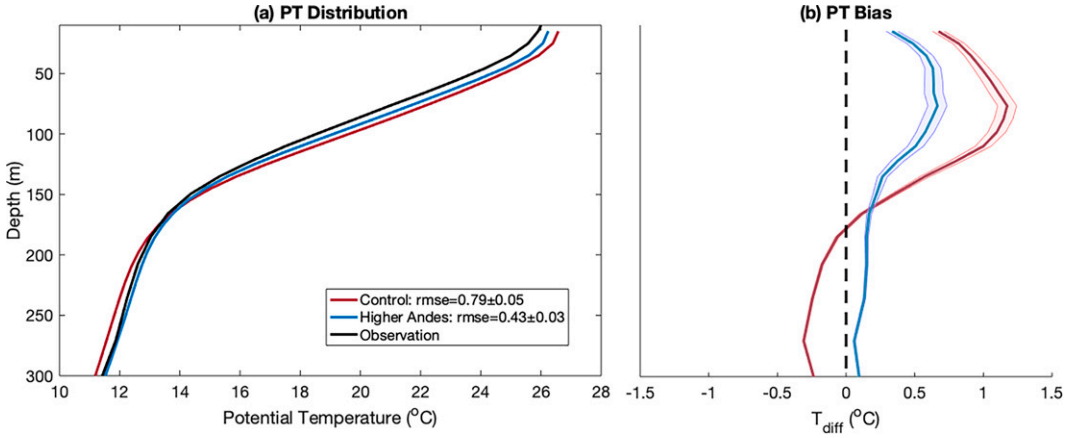

FIG. 5. (a) Vertical distribution of the potential temperature (PT; °C) averaged over the Niño-3 region (5°S–5°N, 150°–90°W). (b) Biases of PT in the vertical distribution over the Niño-3 region (model experiments minus observations). Error bars are calculated with a method similar to that used in Fig. 2.

Fedorov 2020), the modification of the Andes is expected to influence the ENSO cycle. The long-term changes in ocean mean-state climate are the results of the changes in ENSO, as was suggested by Atwood et al. (2017). In the periods during which ENSO has an unusually large amplitude, the mean-state climate will have cooler SSTs in the eastern Pacific and stronger precipitation in the western Pacific, which tends to damp ENSO variability. In fact, the changes in the mean state can affect the major feedbacks that control the characteristics of the ENSO cycle (Karamperidou et al. 2020). Therefore, in this section, we will evaluate ENSO performance in the Higher Andes experiment from various characteristics of the ENSO cycle.

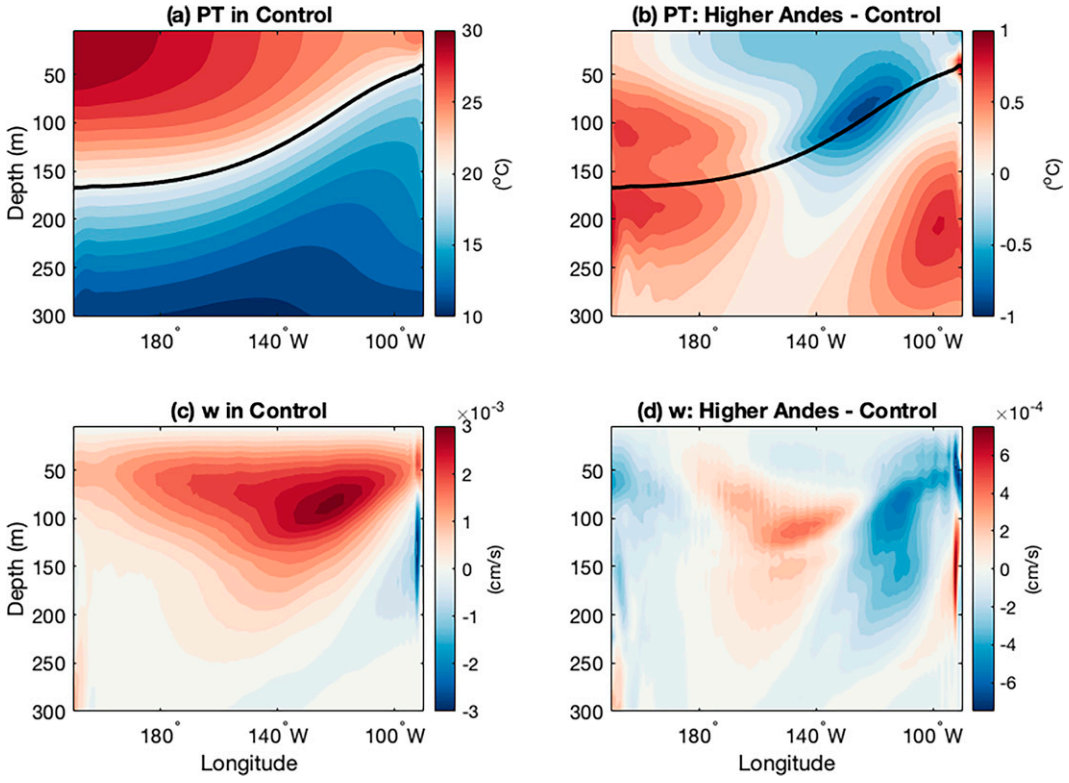

FIG. 6. (a) Vertical PT distribution at the equator for Control experiment (°C), the black line representing the depth of the 20°C isotherm (Z20). (b) PT distribution for Higher Andes minus Control (°C), with the black line representing the same Z20 as in (a). (c) Vertical velocity (w; cm s^{-1}) for Control experiment. (d) Vertical velocity (cm s^{-1}) for Higher Andes minus Control.

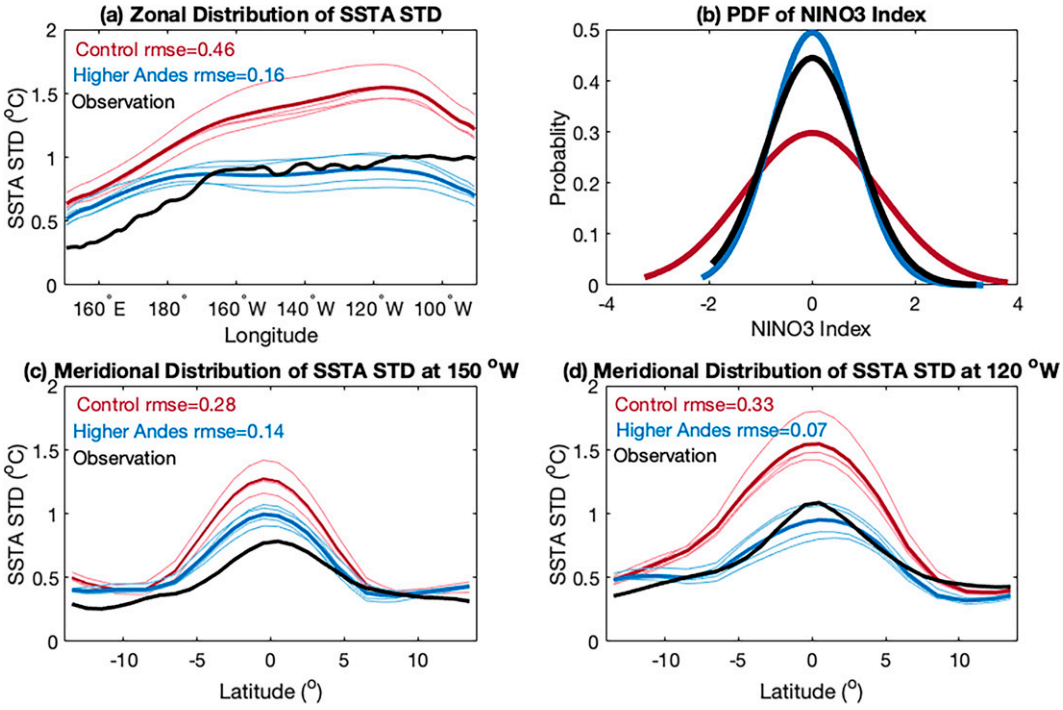

FIG. 7. (a) Standard deviation (STD) of SST anomaly (SSTA) along the equator (°C; 5°S–5°N average). (b) Probability distribution function (PDF) of the Niño-3 index. (c),(d) Meridional distribution of SSTA STD (°) at 150° and 120°W, respectively. The 160-yr model results are divided into four sections of 40 years. Distributions of each section are plotted as thin light lines and the averaged values of the four nonoverlapping sections are plotted as thick dark lines. The legends also show RMSEs calculated between the averaged distributions and the observations. See section 2 for detailed explanations.

a. Amplitude

Figure 7a shows the zonal distribution of the standard deviation (STD) of SST anomalies (SSTA) over the equatorial Pacific. The observation exhibits a small variability in the western Pacific region but from 170°W to the South American coast, the SSTA has a near-constant STD of about 0.9°C. In the Control experiment, the SSTA STD is around 0.5°C larger than observed all along the equator. The simulated SSTA variability also peaks clearly around 115°W before decreasing toward the South American coast. With the Higher Andes setting, the SSTA variability is decreased all over the equatorial Pacific, resulting in a similar amplitude of SSTA STD to the observation from 170° to 120°W. The differences in the variability strength is consistent with changes in the Niño-3 index probability distribution function (PDF) (Fig. 7b). In the Control experiment, extreme El Niño and La Niña events happen more frequently than the observations. But in the Higher Andes experiment, the distribution gets more concentrated to the center and the shape of its PDF is more similar to the observation. Although SSTA variability is still too high in the western equatorial Pacific and now has a too low variability in the far eastern Pacific in the Higher Andes experiment, its RMSE is still much smaller than the Control experiment. Overall, the Higher Andes experiment captures a much weaker SSTA variability over the equatorial Pacific compared with the Control experiment, more consistent with the observed variability.

Figures 7c and 7d show the meridional SSTA STD distributions in the central (150°W) and eastern (120°W) Pacific. In the central Pacific, the Control SSTA variations are much stronger than the observation from the 5°S to 5°N region, with an error of 0.5°C at the equator (66% stronger than the observation). By adjusting the Andes, the difference from the observation is reduced by more than a half and is now down to 0.2°C larger than observed. In the eastern Pacific, the Control experiment has also a too large STD. With Higher Andes the STD is much reduced and the observation falls within uncertainties (blue shading in Fig. 7d). The comparison of the meridional distribution demonstrates that the Higher Andes experiment largely improves the SSTA variation errors near the equator.

In the Niño-3 region, the Higher Andes experiment has slightly weaker SSTA STD (0.8°C) compared to the observation (1.0°C), while the Control experiment variation is about 50% stronger than the observation (1.5°C). The distribution of SSTA in the Niño-3 region is quite narrow in the observation, with 90% of the SSTA being moderate or neutral SSTA (Niño-3 SSTA between −1.5° and +1.5°C). The distribution in the Control experiment is too spread out, with only 72% of moderate or neutral SSTA. In this aspect, the Higher Andes experiment is closer to the observation (94% of moderate or neutral SSTA). The meridional distribution of SSTA is closely related to the frequency of ENSO and the meridional span of the anomalous Bjerknes feedback (e.g., Neale et al. 2008).

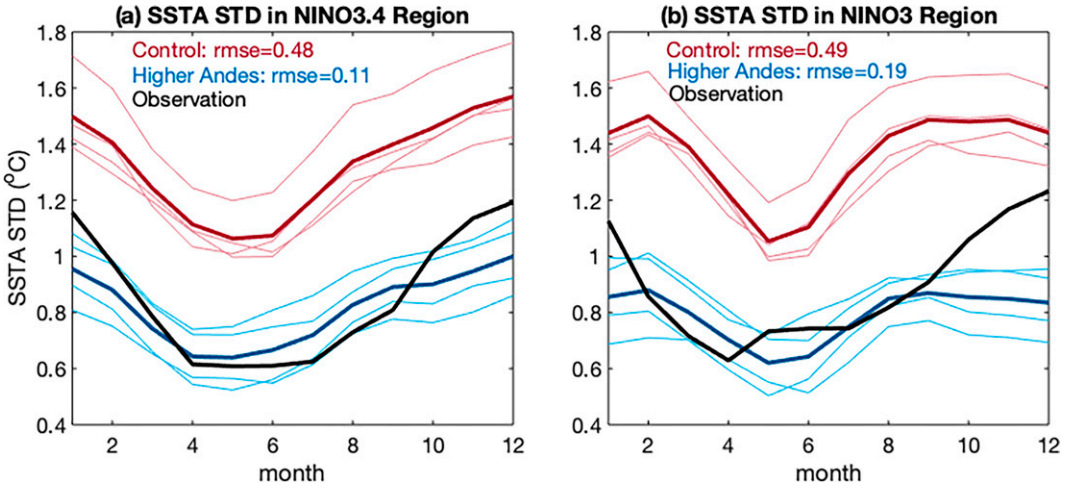

FIG. 8. Seasonal evolution of SSTA STD (°) in the (a) Niño-3.4 region and (b) Niño-3 region.

Figure 8 shows the seasonality of the ENSO variations. ENSO variability peaks during boreal winter and is weakest during boreal spring. This pattern is reproduced by both experiments but the intensity of the variability is too high in the Control experiment and is mostly correct in the Higher Andes experiment (within the observed values; blue lines). A closer analysis shows that the intensity of the seasonality (defined as the variability during November–January divided by March–May) is slightly increased in the Higher Andes experiment compared to the Control experiment and is closer to the observation [Niño-3.4 region (5°N–5°S, 170°–120°W): 1.4 (Higher Andes), 1.3 (Control) and 1.7 (Observation); Niño-3 region: 1.2 (Higher Andes), 1.2 (Control), and 1.7 (Observation)].

b. *Skewness*

The SSTA skewness is a key measurement of the ENSO asymmetry, which is produced by the nonlinear processes in the ENSO cycle (e.g., An et al. 2020). In the eastern Pacific Niño-3 region, the SSTA skewness is strongly positive (Dommenget et al. 2013), meaning that El Niño events can reach larger amplitudes than La Niña events, but occurring less frequently.

Similar to Kohyama et al. (2017), we calculate the skewness of the 11-month running-mean Niño-3 SSTA (Fig. 9a) and find a value of 0.9. The same method is applied to the Control (Fig. 9b) and Higher Andes (Fig. 9c) experiments. In the control experiment, the skewness is less than half of the observed

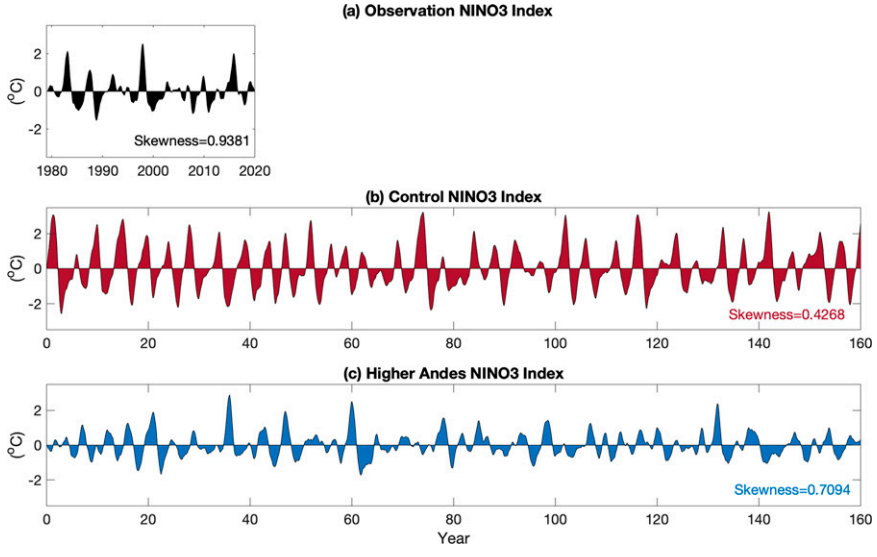

FIG. 9. Time series of 11-month running-mean Niño-3 index, as in Kohyama et al. (2017), for (a) observations, (b) Control, and (c) Higher Andes. Skewness of the distributions indicated at the bottom right of each panel.

(0.4), suggesting that the El Niño and La Niña events are too similar in amplitude. In the Higher Andes experiment, the skewness (0.7) is still too weak but much closer to the observed value. The calculation of the skewness is consistent with the changes in the PDF of the experiments (Fig. 7b). The variation in the observations ranges from −1.94° to 3.19°C. In the Control experiment, the range is −3.26° to 3.81°C, while in the Higher Andes experiment it is −2.14° to 3.33°C. Thus, the Higher Andes experiment captures a more similar variation range and the asymmetry between positive and negative phases.

c. *Spectral characteristics*

The spectra of the Niño-3 index can reveal the variability across time scales of the ENSO cycle (Guilyardi et al. 2009). In the spectrum of the observed Niño-3 index time series, the strongest signal is at 0.27 yr^{-1}, which is a 3.7-yr cycle, but even with this strongest signal its normalized amplitude is only 0.51. The dominant ENSO cycle does not have a very strong signal at a particular frequency; instead, the ENSO cycle is somewhat irregular and its period is around 4 years.

To perform a spectral analysis with uncertainties appropriate for comparison to the observed 40-yr record, we used 160 years of data split into four sections of 40-yr spans of data. The spectrum is calculated for each section (light lines) and then the average at each frequency (bold lines) for the Control and Higher Andes experiments (Fig. 10) are shown. The Control experiment spectrum has an excessive peak at the frequency of 0.22 yr^{-1}, revealing its very strong periodic 4.5-yr cycle, which is contradictory to the observation. A weaker peak near a 10-yr period is also present in the Control experiment, but not in the observation. In the Higher Andes experiment, the 4.5- and 10-yr peaks disappear and the spectrum more realistically captures a 3–8-yr irregular, broadband ENSO cycles. Although the amplitude of the Higher Andes experiment is slightly weaker than the observed spectrum, the observed spectrum falls within the error bars of the Higher Andes experiment in most of the frequencies between 0.1 and 0.4. At higher frequencies (0.5 cycles per year and above), the observations and both simulations agree. The irregularity of ENSO over its dominant frequency range is therefore much improved in the Higher Andes experiment.

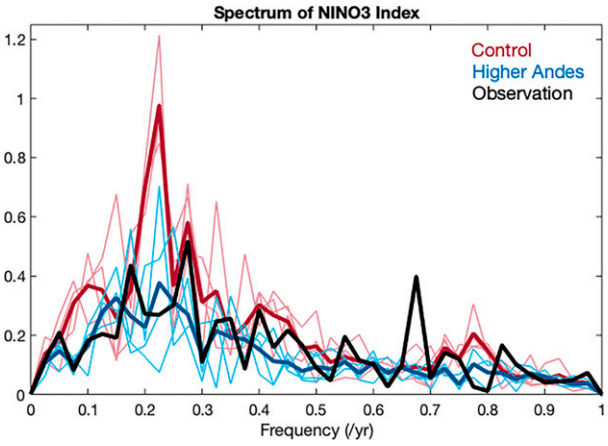

FIG. 10. Normalized spectrum of the Niño-3 index. The 160-yr model results are divided into four nonoverlapping sections of 40 years. The spectrum of each section is plotted as a thin light line and the averaged value of the four sections is plotted as a thick bold lines. See section 2 for detailed explanations.

5. Mechanism

The modification of the Andes results in a more La Niña–like oceanic mean state (steeper thermocline tilt, colder eastern Pacific surface waters, enhanced eastern Pacific zonal and meridional wind stresses), accompanied by fewer, less periodic, meridionally narrower, and less extreme ENSO events with greater asymmetry between El Niño and La Niña. For the changes in the mean state, the mechanisms are similar to what has been discussed in Xu and Lee (2021), with the additional influence of ocean dynamical processes, especially upwelling and horizontal advection. A higher elevation of the Andes has a stronger effect in squeezing the isentropic layers in the atmosphere compared with the Control experiment. As a result, when the midlatitude westerly wind approaches the Andes, it becomes more difficult for the air mass to cross the mountains so the wind turns equatorward. This equatorward turning is accompanied by downward motion because of conservation of potential vorticity. With the strengthening of the anticyclonic motion in the southeast Pacific associated with this equatorward turning, the atmosphere will have lower specific humidity and stronger latent heat uptake, enhancing the formation of the low-level clouds above the ocean. These low-level clouds will block the shortwave radiation and further lower the SST in a positive feedback (Takahashi and Battisti 2007). The thermocline becomes more tilted and the eastern upper Pacific less stratified. The ocean upwelling is weaker in the eastern Pacific and stronger in the central Pacific, consistent with the change in zonal wind stress. These changes in the Higher Andes experiment are correlated with the ENSO variations, either by changing the mean-state feedback or by changing the strength of the correlation between anomalies.

We calculated the Bjerknes index (BJ) as Eq. (1) (Fig. 11), where uncertainty in each terms is estimated based on 1000 samples using the bootstrapping method. Detailed comparisons for each term are shown in Table 1. Results indicate that the reason for the weaker ENSO in the Higher Andes experiment is the stronger damping effect from the mean state. Among the contributions from the different terms, the difference is mainly due to the stronger thermal damping, the stronger mean advection damping, and the weaker thermocline feedback.

The thermal damping term is the linear regression between the surface energy flux anomaly and the eastern Pacific SST anomaly. The surface energy flux depends negatively on the regional SST, and in the Higher Andes experiment this regression has a steeper slope. According to Kim et al. (2014), this atmospheric feedback is underestimated in the CMIP3 and CMIP5 models. In our experiment, the changes in the

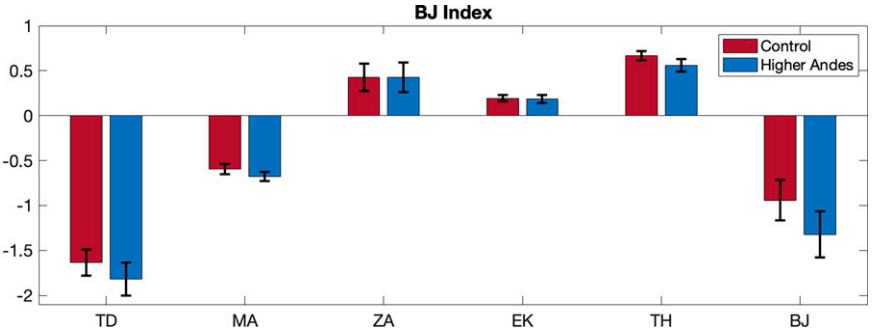

FIG. 11. BJ index in both experiments. Abbreviations are TD: thermal damping; MA: mean advection damping. ZA: zonal advection feedback; EK: Ekman feedback; TH: Thermocline feedback; and BJ: BJ index, the sum of all the previous terms. The error bars represent the 95% confidence level. They are obtained by bootstrapping of the original data 1000 times, calculating the corresponding BJ indexes with each bootstrapping sample, then computing the standard deviations of each term.

regression are mainly contributed by the change in latent heat flux (Table 1). The Higher Andes experiment has stronger downward motion of the air over the southeast Pacific with lowered specific humidity, inducing stronger evaporation and takes up more latent heat flux from the ocean surface. The stronger latent heat flux contributes to a stronger thermal damping. However, this term, estimated by linear regression, has a relatively large uncertainty related to the fact that the thermal damping includes some nonlinear feedback including the subsidence response to SST and the high-level cloud cover. Thus, thermal damping is only moderately stronger in the Higher Andes experiment than in the Control experiment.

The second term that contributes to the stronger damping BJ index is the mean advection damping. Among the three directions, the zonal and meridional mean currents are positive feedback that strengthens the ENSO cycle, but the vertical current has a much stronger negative effect. In the comparison between the Control and the Higher Andes experiments, the changes in all three dimensions are significant (Table 1). The weaker zonal mean current feedback is the main contributing term for the difference between Higher Andes and Control experiments. In the Higher Andes experiment, the mean westward current velocity in the Niño-3 region within the mixed layer decreases from 5.4 to 3.5 cm s^{-1} (36% decrease). This change is consistent with the weaker zonal wind stress in the eastern tropical Pacific region (Fig. 4b).

The third term that contributes the stronger damping is the weakened thermocline feedback in the Higher Andes experiment. The thermocline feedback quantifies the influence from the thermocline depth anomaly to the eastern Pacific surface temperature anomaly. In the Higher Andes experiment, the eastern Pacific becomes colder and the mean thermocline becomes deeper (Fig. 6. As a result, the upper ocean is less stratified in the Niño-3 region (Fig. 5). When the eastern equatorial Pacific becomes less stratified, the zonal thermocline slope is less sensitive to the wind stress (Kim et al. 2014) (β_h in Table 1). With the weaker oceanic response to the wind anomaly in the Higher Andes experiment, the thermocline feedback becomes weaker and results in a weaker ENSO cycle.

Combining all the terms of the BJ index, the average damping index changed by 38%, from −0.94 in the Control experiment to −1.31 in the Higher Andes experiment. Therefore, it is very likely that the ENSO amplitude is weaker in the Higher Andes experiment because of the stronger overall damping effect.

6. Conclusions

In this study, we performed an experiment to understand how the simulated height of the Andes affects the Pacific climate of the CESM atmosphere–ocean global coupled model. The results show that by elevating the height of the Andes, the model simulates the tropical Pacific mean-state climate and the ENSO variations better, which suggests that creating elevation maps by simply smoothing away the high and low features of high-resolution observations is an oversimplification. For the mean-state climate, the Higher Andes experiment results in a greater east–west and north–south SST gradient, and reduced precipitation over the South Pacific. Easterly wind stress in the eastern and central Pacific becomes stronger, accompanied by stronger cross-equator southerly wind stress. In the upper ocean, the Higher Andes experiment is less stratified over the eastern tropical Pacific, and it has a steeper east–west thermocline slope. ENSO variability is strongly affected: the Higher Andes experiment exhibits a smaller amplitude, a greater skewness and a less regular ENSO period. All of these changes exceeded the uncertainty due to limited simulation length, and all are more consistent with observations results. Therefore, in this version of CESM a higher elevation of the Andes allows better simulation of the tropical Pacific mean state as well as ENSO variations in the CESM coupled model.

Although the improvement in the mean-state climate and the ENSO properties are related, it is hard to distinguish cause

TABLE 1. BJ index equation [Eq. (1)] terms comparison. Terms with boldface values do not overlap in the 33%–67% range (1 STD) between the two experiments, which means the change is significant. An asterisk (*) indicates terms that are not directly included in the BJ index equation. C_{time} is the time constant that converts the unit from s^{-1} to yr^{-1}.

Name	Decomposition of the term	Definition	Control	Higher Andes
TD	$-\alpha_s$	$Q_s = -\alpha_s\langle T'\rangle$	**−1.64**	**−1.82**
	$-\alpha_{\text{SW}}$*	$\text{SW}_s = -\alpha_{\text{SW}}\langle T'\rangle$	**−0.40**	**−0.23**
	$-\alpha_{\text{LW}}$*	$\text{LW}_s = -\alpha_{\text{LW}}\langle T'\rangle$	−0.05	−0.05
	$-\alpha_{\text{LH}}$*	$\text{LH}_s = -\alpha_{\text{LH}}\langle T'\rangle$	**−1.08**	**−1.41**
	$-\alpha_{\text{SH}}$*	$\text{SH}_s = -\alpha_{\text{SH}}\langle T'\rangle$	−0.12	−0.13
MA			**−0.59**	**−0.68**
	Udamp	$-\dfrac{\langle\overline{u}\rangle}{L_x}$	**0.36**	**0.26**
	Vdamp	$-\dfrac{\langle -2y\overline{v}\rangle}{L_y^2}$	**0.49**	**0.46**
	Wdamp	$-\dfrac{\langle\mathcal{H}(\overline{w})\overline{w}\rangle}{H_m}$	**−1.45**	**−1.40**
ZA			0.43	0.44
	μ_a	$[\tau_x'] = \mu_a\langle T'\rangle$	5.36×10^{-3}	5.29×10^{-3}
	β_u	$\langle u'\rangle = \beta_u[\tau_x']$	4.26	4.85
	$\left\langle\dfrac{\partial\overline{T}}{\partial x}\right\rangle \times C_{\text{time}}$		**18.63**	**16.97**
EK			0.20	0.19
	μ_a	$[\tau_x'] = \mu_a\langle T'\rangle$	5.36×10^{-3}	5.29×10^{-3}
	β_w	$\langle\mathcal{H}(\overline{w})w'\rangle = -\beta_w[\tau_x']$	2.50×10^{-5}	2.37×10^{-5}
	$\left\langle\dfrac{\partial\overline{T}}{\partial z}\right\rangle \times C_{\text{time}}$		1.46×10^{6}	1.50×10^{6}
TH			**0.67**	**0.56**
	μ_a	$[\tau_x'] = \mu_a\langle T'\rangle$	5.36×10^{-3}	5.29×10^{-3}
	β_h	$\langle h'\rangle = \beta_h[\tau_x']$	**5.71**	**5.09**
	a_h	$\langle\mathcal{H}(\overline{w})T_{50\text{m}}'\rangle = a_h\langle h'\rangle$	17.93	17.44
	$\left\langle\dfrac{\overline{w}}{H_m}\right\rangle \times C_{\text{time}}$		1.22	1.19
BJ			**−0.94**	**−1.31**

and effect. On the one hand, the changes in the climate mean state can influence the ENSO characteristics (e.g., Fedorov and Philander 2000; Hu and Fedorov 2018; Zhao and Fedorov 2020). Zhao and Fedorov (2020), suggesting that strengthening of thermocline stratification and deepening the mean thermocline depth will produce stronger ENSO. In our simulations, the Higher Andes experiment has a weaker upper-ocean stratification and a shallower thermocline depth over the central and eastern Pacific (Fig. 6), and we found a consistent change toward weaker ENSO events (Fig. 7). In addition, Hu and Fedorov (2018) suggest that with a stronger zonal wind over the central-western Pacific and stronger cross-equatorial winds over the eastern Pacific, there will be a weaker amplitude of ENSO variations. Consistently, our results also suggest that the elevation of the Andes strengthens the wind and weakens ENSO variability. On the other hand, the changes in the ENSO variations can also influence the tropical Pacific mean state. Because of the asymmetry of El Niño and La Niña, the changes of the mean state can result from the varying occurrence and strength of strong El Niño and La Niña events, and the residual between them (Rodgers et al. 2004; McPhaden et al. 2011; Atwood et al. 2017). In our result, the Higher Andes experiment significantly reduces the occurrence of strong El Niño events, but has a smaller influence on the La Niña events (Fig. 9). As a result, the eastern Pacific will have a cooler mean state in the Higher Andes case.

Feng and Poulsen (2014) performed a similar experiment of modifying the height of the Andes in a similar global coupled climate model (CCSM4), and examined the response of the Pacific climate. However, their purpose was to understand the impact of Andean uplift over geological time, while our purpose was to understand biases in the modern Pacific climate and ENSO. Furthermore, the details of how the Andes were changed and thus the results are quite different. Feng and Poulsen (2014) carried out their experiment to understand if the long-term climate transition in the Pacific since the late Cenozoic is the result from 1- to 3-km uplift of the central Andes. Our experiment is seeking an appropriate representation of the

Andes in global climate models for the present day (changing the maximum elevation from about 2 km to about 5 km), so as to understand the model biases in the Pacific climate simulation. With this purpose, we compare our results against observations to evaluate the simulation's performance. In addition, the resulting changes in ENSO here are distinct from Feng and Poulsen (2014). In their experiment, as the height of the Andes increases, the ENSO period decreases. In comparison, here no obvious change in the dominant frequency occurs, but the strength of the Niño-3 index spectral band reduces in our Higher Andes experiment (Fig. 10). In their histogram of ENSO events, they have slightly more extreme El Niño and La Niña events, less moderate El Niño and La Niña events and weaker El Niño and La Niña events in the Higher Andes experiment. In our result, both extreme and moderate El Niño and La Niña events decreased in frequency in the Higher Andes experiment (Fig. 7b), and phase asymmetry increased. However, consistent with our results, they find that the mean zonal SST gradient increased with increasing the height of the Andes, although more so than in our experiment. They found major strengthening of zonal winds while we find modest changes to the mean wind magnitude and structure.

Overall, we consider the modification of the Andes an improvement in representing the South American topography and the tropical Pacific mean climate and its variability. This work highlights the fact that increasing the resolution of a climate model without addressing the height of the Andes could be problematic.

Acknowledgments. We want to thank Dr. Alexey Fedorov, Anson Cheung, and Mengxi Wu for their comments and suggestions on this research. The constructive comments from three anonymous reviewer are also greatly appreciated. The runs are performed on the Brown Ocean State Center for Advanced Resources (OSCAR). We want to thank the Institute at Brown for Environment and Society (IBES) for supporting this project on the AGU 2022 Ocean Science presentation. BFK was supported by ONR N00014-17-1-2393. MJM is supported by NOAA's Global Ocean Monitoring and Observing Program. This is PMEL contribution number 5304.

Data availability statement. Model results are available at https://doi.org/10.7910/DVN/3H1E4X.

REFERENCES

Abellán, E., S. McGregor, and M. H. England, 2017: Analysis of the southward wind shift of ENSO in CMIP5 models. *J. Climate*, **30**, 2415–2435, https://doi.org/10.1175/JCLI-D-16-0326.1.

Adler, R. F., and Coauthors, 2003: The version-2 Global Precipitation Climatology Project (GPCP) monthly precipitation analysis (1979–present). *J. Hydrometeor.*, **4**, 1147–1167, https://doi.org/10.1175/1525-7541(2003)004<1147:TVGPCP>2.0.CO;2.

An, S.-I., E. Tziperman, Y. M. Okumura, and T. Li, 2020: ENSO irregularity and asymmetry. *El Niño Southern Oscillation in a Changing Climate*. *Geophys. Monogr.*, Vol. 253, Amer. Geophys. Union, 153–172, https://doi.org/10.1002/9781119548164.ch7.

Atwood, A. R., D. S. Battisti, A. T. Wittenberg, W. H. G. Roberts, and D. J. Vimont, 2017: Characterizing unforced multi-decadal variability of ENSO: A case study with the GFDL CM2.1 coupled GCM. *Climate Dyn.*, **49**, 2845–2862, https://doi.org/10.1007/s00382-016-3477-9.

Bastianin, A., A. Lanza, and M. Manera, 2018: Economic impacts of El Niño southern oscillation: Evidence from the Colombian coffee market. *Agric. Econ.*, **49**, 623–633, https://doi.org/10.1111/agec.12447.

Bayr, T., M. Latif, D. Dommenget, C. Wengel, J. Harlaß, and W. Park, 2018: Mean-state dependence of ENSO atmospheric feedbacks in climate models. *Climate Dyn.*, **50**, 3171–3194, https://doi.org/10.1007/s00382-017-3799-2.

Bellenger, H., E. Guilyardi, J. Leloup, M. Lengaigne, and J. Vialard, 2014: ENSO representation in climate models: From CMIP3 to CMIP5. *Climate Dyn.*, **42**, 1999–2018, https://doi.org/10.1007/s00382-013-1783-z.

Bjerknes, J., 1969: Atmospheric teleconnections from the equatorial Pacific. *Mon. Wea. Rev.*, **97**, 163–172. https://doi.org/10.1175/1520-0493(1969)097<0163:ATFTEP>2.3.CO;2.

Boos, W. R., and Z. Kuang, 2010: Dominant control of the South Asian monsoon by orographic insulation versus plateau heating. *Nature*, **463**, 218–222, https://doi.org/10.1038/nature08707.

Brown, J. R., and Coauthors, 2020: Comparison of past and future simulations of ENSO in CMIP5/PMIP3 and CMIP6/PMIP4 models. *Climate Past*, **16**, 1777–1805, https://doi.org/10.5194/cp-16-1777-2020.

Burls, N. J., L. Muir, E. M. Vincent, and A. Fedorov, 2017: Extra-tropical origin of equatorial Pacific cold bias in climate models with links to cloud albedo. *Climate Dyn.*, **49**, 2093–2113, https://doi.org/10.1007/s00382-016-3435-6.

Cai, W., and Coauthors, 2018: Increased variability of eastern Pacific El Niño under greenhouse warming. *Nature*, **564**, 201–206, https://doi.org/10.1038/s41586-018-0776-9.

——, and Coauthors, 2021: Changing El Niño–southern oscillation in a warming climate. *Nat. Rev. Earth Environ.*, **2**, 628–644, https://doi.org/10.1038/s43017-021-00199-z.

Cane, M. A., and S. E. Zebiak, 1985: A theory for El Niño and the southern oscillation. *Science*, **228**, 1085–1087, https://doi.org/10.1126/science.228.4703.1085.

Dommenget, D., T. Bayr, and C. Frauen, 2013: Analysis of the non-linearity in the pattern and time evolution of El Niño Southern Oscillation. *Climate Dyn.*, **40**, 2825–2847, https://doi.org/10.1007/s00382-012-1475-0.

Fang, K., and Coauthors, 2021: ENSO modulates wildfire activity in China. *Nat. Commun.*, **12**, 1764, https://doi.org/10.1038/s41467-021-21988-6.

Fedorov, A. V., and S. G. Philander, 2000: Is El Niño changing? *Science*, **288**, 1997–2002, https://doi.org/10.1126/science.288.5473.1997.

Feng, R., and C. J. Poulsen, 2014: Andean elevation control on tropical Pacific climate and ENSO. *Paleoceanogr. Paleoclimatol.*, **29**, 795–809, https://doi.org/10.1002/2014PA002640.

Fox-Kemper, B., S. Bachman, B. Pearson, and S. Reckinger, 2014: Principles and advances in subgrid modeling for eddy-rich simulations. *CLIVAR Exchanges*, No. 65, International CLIVAR Project Office, Southampton, United Kingdom, 42–46.

Good, S. A., M. J. Martin, and N. A. Rayner, 2013: EN4: Quality controlled ocean temperature and salinity profiles and monthly objective analyses with uncertainty estimates. *J. Geophys. Res. Oceans*, **118**, 6704–6716, https://doi.org/10.1002/2013JC009067.

Guilyardi, E., A. Wittenberg, A. Fedorov, C. Collins, A. Capotondi, G. J. Van Oldenborgh, and T. Stockdale, 2009: Understanding

El Niño in ocean–atmosphere general circulation models: Progress and challenges. *Bull. Amer. Meteor. Soc.*, **90**, 325–340, https://doi.org/10.1175/2008BAMS2387.1.

——, A. Capotondi, M. Lengaigne, S. Thual, and A. T. Wittenberg, 2020: ENSO modeling. *El Niño Southern Oscillation in a Changing Climate*, *Geophys. Monogr.*, Vol. 253, Amer. Geophys. Union, 199–226, https://doi.org/10.1002/9781119548164.ch9.

Haine, T. W. N., and Coauthors, 2021: Is computational oceanography coming of age? *Bull. Amer. Meteor. Soc.*, **102**, E1481–E1493, https://doi.org/10.1175/BAMS-D-20-0258.1.

He, J., N. C. Johnson, G. A. Vecchi, B. Kirtman, A. T. Wittenberg, and S. Sturm, 2018: Precipitation sensitivity to local variations in tropical sea surface temperature. *J. Climate*, **31**, 9225–9238, https://doi.org/10.1175/JCLI-D-18-0262.1.

Hu, S., and A. V. Fedorov, 2018: Cross-equatorial winds control El Niño diversity and change. *Nat. Climate Change*, **8**, 798–802, https://doi.org/10.1038/s41558-018-0248-0.

Hurrell, J. W., and Coauthors, 2013: The Community Earth System Model: A framework for collaborative research. *Bull. Amer. Meteor. Soc.*, **94**, 1339–1360, https://doi.org/10.1175/BAMS-D-12-00121.1.

Jin, F.-F., 1996: Tropical ocean–atmosphere interaction, the Pacific cold tongue, and the El Niño-Southern Oscillation. *Science*, **274**, 76–78, https://doi.org/10.1126/science.274.5284.76.

——, 1997a: An equatorial ocean recharge paradigm for ENSO. Part I: Conceptual model. *J. Atmos. Sci.*, **54**, 811–829, https://doi.org/10.1175/1520-0469(1997)054<0811:AEORPF>2.0.CO;2.

——, 1997b: An equatorial ocean recharge paradigm for ENSO. Part II: A stripped-down coupled model. *J. Atmos. Sci.*, **54**, 830–847, https://doi.org/10.1175/1520-0469(1997)054<0830:AEORPF>2.0.CO;2.

——, S. T. Kim, and L. Bejarano, 2006: A coupled-stability index for ENSO. *Geophys. Res. Lett.*, **33**, L23708, https://doi.org/10.1029/2006GL027221.

——, H.-C. Chen, S. Zhao, M. Hayashi, C. Karamperidou, M. F. Stuecker, R. Xie, and L. Geng, 2020: Simple ENSO models. *El Niño Southern Oscillation in a Changing Climate*, *Geophys. Monogr.*, Vol. 253, Amer. Geophys. Union, 119–151, https://doi.org/10.1002/9781119548164.ch6.

Karamperidou, C., and Coauthors, 2020: ENSO in a changing climate. *El Niño Southern Oscillation in a Changing Climate*, *Geophys. Monogr.*, Vol. 253, Amer. Geophys. Union, 471–484, https://doi.org/10.1002/9781119548164.ch21.

Kim, S. T., W. Cai, F.-F. Jin, and J.-Y. Yu, 2014: ENSO stability in coupled climate models and its association with mean state. *Climate Dyn.*, **42**, 3313–3321, https://doi.org/10.1007/s00382-013-1833-6.

Kitoh, A., 2007: ENSO modulation by mountain uplift. *Climate Dyn.*, **28**, 781–796, https://doi.org/10.1007/s00382-006-0209-6.

Kohyama, T., D. L. Hartmann, and D. S. Battisti, 2017: La Niña–like mean-state response to global warming and potential oceanic roles. *J. Climate*, **30**, 4207–4225, https://doi.org/10.1175/JCLI-D-16-0441.1.

Lehodey, P., and Coauthors, 2020: ENSO impact on marine fisheries and ecosystems. *El Niño Southern Oscillation in a Changing Climate*, *Geophys. Monogr.*, Vol. 253, Amer. Geophys. Union, 429–451, https://doi.org/10.1002/9781119548164.ch19.

Levine, A., F. F. Jin, and M. J. McPhaden, 2016: Extreme noise–extreme El Niño: How state-dependent noise forcing creates El Niño–La Niña asymmetry. *J. Climate*, **29**, 5483–5499, https://doi.org/10.1175/JCLI-D-16-0091.1.

Lin, J.-L., 2007: The double-ITCZ problem in IPCC AR4 coupled GCMs: Ocean–atmosphere feedback analysis. *J. Climate*, **20**, 4497–4525, https://doi.org/10.1175/JCLI4272.1.

McPhaden, M. J., T. Lee, and D. McClurg, 2011: El Niño and its relationship to changing background conditions in the tropical Pacific Ocean. *Geophys. Res. Lett.*, **38**, L15709, https://doi.org/10.1029/2011GL048275.

——, ——, S. Fournier, and M. A. Balmaseda, 2020: ENSO observations. *El Niño Southern Oscillation in a Changing Climate*, *Geophys. Monogr.*, Vol. 126, Amer. Geophys. Union, 39–63, https://doi.org/10.1002/9781119548164.ch3.

Naiman, Z., P. J. Goodman, J. P. Krasting, S. L. Malyshev, J. L. Russell, R. J. Stouffer, and A. T. Wittenberg, 2017: Impact of mountains on tropical circulation in two Earth system models. *J. Climate*, **30**, 4149–4163, https://doi.org/10.1175/JCLI-D-16-0512.1.

Neale, R. B., J. H. Richter, and M. Jochum, 2008: The impact of convection on ENSO: From a delayed oscillator to a series of events. *J. Climate*, **21**, 5904–5924, https://doi.org/10.1175/2008JCLI2244.1.

Nicholls, N., 1991: The El Niño/southern oscillation and Australian vegetation. *Vegetatio*, **91**, 23–36, https://doi.org/10.1007/BF00036045.

Oueslati, B., and G. Bellon, 2015: The double ITCZ bias in CMIP5 models: Interaction between SST, large-scale circulation and precipitation. *Climate Dyn.*, **44**, 585–607, https://doi.org/10.1007/s00382-015-2468-6.

Philander, S. G. H., D. Gu, G. Lambert, T. Li, D. Halpern, N.-C. Lau, and R. C. Pacanowski, 1996: Why the ITCZ is mostly north of the equator. *J. Climate*, **9**, 2958–2972, https://doi.org/10.1175/1520-0442(1996)009<2958:WTIIMN>2.0.CO;2.

Planton, Y. Y., and Coauthors, 2021: Evaluating climate models with the CLIVAR 2020 ENSO metrics package. *Bull. Amer. Meteor. Soc.*, **102**, E193–E217, https://doi.org/10.1175/BAMS-D-19-0337.1.

Praveen Kumar, B., J. Vialard, M. Lengaigne, V. S. N. Murty, and M. J. McPhaden, 2012: TropFlux: Air-sea fluxes for the global tropical oceans—Description and evaluation. *Climate Dyn.*, **38**, 1521–1543, https://doi.org/10.1007/s00382-011-1115-0.

——, ——, ——, ——, ——, M. F. Cronin, F. Pinsard, and K. Gopala Reddy, 2013: TropFlux wind stresses over the tropical oceans: Evaluation and comparison with other products. *Climate Dyn.*, **40**, 2049–2071, https://doi.org/10.1007/s00382-012-1455-4.

Prieto, M. D. R., 2007: ENSO signals in South America: Rains and floods in the Paraná River region during colonial times. *Climatic Change*, **83**, 39–54, https://doi.org/10.1007/s10584-006-9188-1.

Rayner, N. A., D. E. Parker, E. B. Horton, C. K. Folland, L. V. Alexander, D. P. Rowell, E. C. Kent, and A. Kaplan, 2003: Global analyses of sea surface temperature, sea ice, and night marine air temperature since the late nineteenth century. *J. Geophys. Res.*, **108**, 4407, https://doi.org/10.1029/2002JD002670.

Rodgers, K. B., P. Friederichs, and M. Latif, 2004: Tropical Pacific decadal variability and its relation to decadal modulations of ENSO. *J. Climate*, **17**, 3761–3774, https://doi.org/10.1175/1520-0442(2004)017<3761:TPDVAI>2.0.CO;2.

Takahashi, K., and D. S. Battisti, 2007: Processes controlling the mean tropical Pacific precipitation pattern. Part II: The SPCZ and the southeast Pacific dry zone. *J. Climate*, **20**, 5696–5706, https://doi.org/10.1175/2007JCLI1656.1.

Wengel, C., M. Latif, W. Park, J. Harlaß, and T. Bayr, 2018: Seasonal ENSO phase locking in the Kiel climate model: The

importance of the equatorial cold sea surface temperature bias. *Climate Dyn.*, **50**, 901–919, https://doi.org/10.1007/s00382-017-3648-3.

Wittenberg, A. T., and Coauthors, 2018: Improved simulations of tropical Pacific annual-mean climate in the GFDL FLOR and HiFLOR coupled GCMs. *J. Adv. Model. Earth Syst.*, **10**, 3176–3220, https://doi.org/10.1029/2018MS001372.

Wyrtki, K., 1985: Water displacements in the Pacific and the genesis of El Niño cycles. *J. Geophys. Res.*, **90**, 7129–7132, https://doi.org/10.1029/JC090iC04p07129.

Xu, W., and J.-E. Lee, 2021: The Andes and the southeast Pacific cold tongue simulation. *J. Climate*, **34**, 415–425, https://doi.org/10.1175/JCLI-D-19-0901.1.

Zhang, T., and D.-Z. Sun, 2014: ENSO asymmetry in CMIP5 models. *J. Climate*, **27**, 4070–4093, https://doi.org/10.1175/JCLI-D-13-00454.1.

Zhao, B., and A. Fedorov, 2020: The effects of background zonal and meridional winds on ENSO in a coupled GCM. *J. Climate*, **33**, 2075–2091, https://doi.org/10.1175/JCLI-D-18-0822.1.